



## Adsorption of octanohydroxamic acid at fluorite surface in presence of calcite species

Zhou-jie WANG<sup>1</sup>, Long-hua XU<sup>1,2</sup>, Hou-qin WU<sup>1</sup>, Huan ZHOU<sup>1</sup>,  
Jin-ping MENG<sup>1</sup>, Xiao-mei HUO<sup>1</sup>, Ling-yun HUANG<sup>3</sup>

1. Key Laboratory of Solid Waste Treatment and Resource Recycle, Ministry of Education, Southwest University of Science and Technology, Mianyang 621010, China;
2. State Key Laboratory for Environment-friendly Energy Materials, Southwest University of Science and Technology, Mianyang 621010, China;
3. State Key Laboratory of Complex Nonferrous Metal Resources Clean Utilization, Kunming University of Science and Technology, Kunming 650093, China

Received 30 October 2020; accepted 28 June 2021

**Abstract:** The surface properties of fluorite are often affected by dissolved gangue species (e.g., calcite) during the flotation process. Microflotation testing with and without the addition of calcite supernatant was conducted using octanohydroxamic acid (OHA) as the collector. The results revealed that dissolved calcite species significantly affected the flotation behavior of fluorite. Fourier transform infrared spectra confirmed that the decrease in flotation recovery was linked to lower OHA adsorption. Solution chemistry analysis indicated that  $\text{CaCO}_3$  and  $\text{Ca}^{2+}$  from the calcite supernatant were the most favorably adsorbed species, and X-ray photoelectron spectroscopy analysis confirmed the surface adsorption of calcite species. Density functional theory simulations provided a detailed analysis of the multidentate adsorption configuration of OHA, which was the most favorable for adsorption on the fluorite surface. The adsorption energy calculation showed that the calcite dissolved species were more stably adsorbed on the fluorite surface than OHA. The pre-adsorption of calcite dissolved species hindered the adsorption of OHA due to electrostatic repulsion.

**Key words:** fluorite; calcite; flotation; dissolved species; DFT calculation

### 1 Introduction

Fluorite ( $\text{CaF}_2$ ) is a non-renewable natural resource and one of the most important industrial sources of fluorine particularly in the fields of optics, metallurgy, and refrigeration [1]. However, high demand has led to a rapid decline in fluorite reserves. Flotation processing is widely applied to separating fluorite from other co-existing minerals such as calcite ( $\text{CaCO}_3$ ), a low-value gangue mineral [2]. Froth flotation combines physical and chemical separation technologies, where differences

in surface properties allow for the separation of unwanted and valuable minerals [3]. Fatty acid derivatives (e.g., sodium oleate) are the most widely used collectors in the fluorite flotation process; however, the weak steric hindrance of the alkyl chains can lower their selectivity. Thus, hydroxamate type collectors gained popularity due to their superior selectivity toward some metal minerals [4], which is attributed to a more stable chelate formation with metal cations compared to fatty acid collectors [5]. Hydroxamates interact with metal-hydroxylated species at the mineral–water interface, thereby rendering the mineral to be

hydrophobic [6]. Nowadays, two hydroxamate types of collectors were widely used in fluorite flotation: benzhydroxamic acid (BHA;  $C_7H_7NO_2$ ) and octanohydroxamic acid (OHA;  $C_8H_{17}NO_2$ ) [7]. Although both collectors show excellent selectivity in fluorite flotation, BHA is a weaker collector than OHA. Therefore, the OHA was selected as a collector in this study. Additionally, the practical implementation of fluorite flotation separation is affected by the co-existence of various ions in the flotation pulp.

Fluorite and associated gangue, including calcite and barite ( $BaSO_4$ ), are generally semi-soluble salt-type minerals [8]. Thus, these minerals have similar surface properties, and chemical reactivity with reagents; they are also sparingly soluble in water and comprise complex dissolved components [9,10]. The dissolution of gangue can lead to the formation of various metal cations and inorganic anions that adsorb or precipitate on the surface of valuable minerals. This can negatively affect the floatability of the valuable minerals and the adsorption behavior of reagents. Although previous studies have explored the effects of dissolved mineral species associated with semi-soluble gangue minerals on mineral flotation [11], flotation systems involving fluorite have not yet been investigated thoroughly. A previous study on the use of BHA for the separation of fluorite and calcite reported good fluorite recovery under alkaline pH conditions [12]. However, the study only investigated single mineral flotation, and did not account for the effect of dissolved mineral species from calcite. Previous studies by the current authors found that calcium and barium ions dissolved from the lattice of calcite, fluorite and barite surfaces were adsorbed or precipitated at the surface of bastnaesite, which negatively affected the mineral floatability and the adsorption of the collector in the sodium oleate system [13,14].

Traditional mineral surface testing methods cannot be easily applied to exploring the interaction mechanism between reagents and the mineral/water interface on the nanoscale [15]. Thus, computer simulation methods, including density functional theory (DFT) calculations, are valuable tools that provide an in-depth understanding of the interactions, energetic properties and structural properties of adsorbate molecules on the surface of

minerals. DFT simulations could also provide further insights into mineral flotation behavior in various solution environments, which cannot be directly studied experimentally [16,17]. DFT calculations have been used in previous studies on fluorite flotation, and have focused on flotation separation from gangue and adsorption behavior. However, the effect of dissolved gangue species using OHA as a collector remains largely unknown.

This study aimed to investigate the effect of dissolved calcite species on fluorite during fluorite flotation separation using OHA as a collector. The hydrophobicity and interactions were evaluated on a molecular scale. Microflotation testing, Fourier transform infrared (FTIR) spectroscopy, and X-ray photoelectron spectroscopy (XPS) were conducted to study the adsorption of the dissolved calcite species and collector at the surface of fluorite. Simulations based on DFT calculations were used to investigate the adsorption energy and structural changes of OHA in the absence and presence of dissolved calcite species on the fluorite surface. The effect of other variables was minimized by preparing a calcite supernatant to simulate the real solution environment during flotation. The present results would be useful for understanding the effect mechanism of gangue dissolved species in the flotation of fluorite and for further improving the sustainability of mineral processing operations.

## 2 Experimental

### 2.1 Materials and reagents

Fluorite and calcite were obtained from Tongliang in Chongqing, China. The minerals were sieved to remove particles coarser than 0.075 mm (200 mesh) for microflotation testing and XPS analysis. The X-ray diffraction (XRD) patterns (Fig. 1) and chemical composition analysis (Table 1) confirmed the high purity of the fluorite and calcite samples, which was suitable for microflotation testing and analytical measurements. The FTIR spectroscopy fluorite samples were ground to a particle size of  $\sim 5 \mu m$  using an agate mortar at 25 °C. Sodium chloride (supporting electrolyte), ethanol (cleaning solvent), sodium hydroxide (pH regulator), and hydrochloric acid (pH regulator) were obtained from Sinopharm (China). OHA was obtained from Macklin (China). All reagents were of analytical grade.

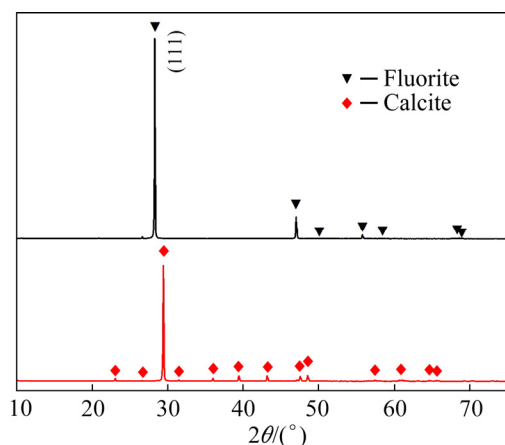


**Fig. 1** X-ray diffraction patterns of fluorite and calcite

**Table 1** Chemical compositions of purified mineral samples (wt.%)

Sample	Ca	F	Si	Al	Na	Mg
Fluorite	70.99	26.39	2.40	0.17	0.02	0.01
Sample	CaO	SiO <sub>2</sub>	MgO	Fe <sub>2</sub> O <sub>3</sub>	BaO	Al <sub>2</sub> O <sub>3</sub>
Calcite	98.32	0.90	0.35	0.11	0.09	0.09

## 2.2 Calcite supernatant preparation

Sieved calcite (200 mesh) was dispersed to a concentration of 5.0 wt.% in ultrapure water obtained from the Milli-Q ultrapure water system (Millipore, Billerica, MA, USA). The suspension was mixed for 1 h using a magnetic stirrer, left to precipitate for 30 min, and filtered using filter paper to obtain a supernatant. The supernatant was centrifuged and filtered using a 0.02 μm syringe filter. The calcium and carbonate ion contents of the calcite supernatant were  $4.5 \times 10^{-6}$  and  $44.8 \times 10^{-6}$ , respectively, as determined using inductively coupled plasma optical emission spectrometry (ICP-OES, Perkin-Elmer OPTIMA8300, Waltham, MA, USA). Supernatant preparation was conducted at 25 °C.

## 2.3 Microflotation experiments

Microflotation was conducted in an XFG-type laboratory flotation machine (Jilin Prospecting Machinery Factory, China) using a 40 mL Plexiglass cell and impeller speed of 1700 r/min.

Sieved fluorite (200 mesh) (2 g) was added to a flotation cell containing either ultrapure water or calcite supernatant, and then the HCl or NaOH was added to the pulp to achieve the desired pH for 7 min. The cell was scraped for 5 min, and the

products were filtered, dried, and weighed. Flotation recovery was calculated based on the particle mass distribution in the floated and non-floated fractions. Microflotation testing was conducted in triplicate for each sample, and the mean value was reported.

## 2.4 FTIR spectra measurements

FTIR spectra were obtained using a Spectrum One FTIR spectrometer (Version BM, Perkin Elmer Instrument Co., USA) in a spectral range of 400 to 4000  $\text{cm}^{-1}$ . The solid microflotation solid samples (particle size of ~5 μm) were washed at least three times with ultrapure water, adjusted to a pH of 9, and vacuum dried at 40 °C for 24 h. The mass ratio of fluorite to KBr was ~1:300. The FTIR spectra were acquired at 25 °C.

## 2.5 XPS measurements

XPS was performed using an ESCALAB 250XI instrument (Thermo Fisher Scientific Inc., USA) equipped with an Al  $K_{\alpha}$  X-ray source, where the binding energies and distribution densities of elements on the sample surface were measured. Sieved samples of fluorite (200 mesh) were outgassed and dried in a vacuum drying oven at 40 °C for 72 h. Survey spectra were recorded in a single sweep from 0 to 1350 eV using a step size of 1.0 eV. Additionally, a step size of 0.1 eV was used for high-resolution elemental scans. The C 1s peak at 284.8 eV (C—C) was used as the internal binding energy standard for calibration, which was fitted using Thermo Fisher Scientific Advantage 5.52 software (Thermo Fisher Scientific Inc., USA).

## 2.6 DFT simulations

The surface reactivity and flotation behavior of minerals are predominantly governed by the characteristics of the most commonly exposed surface of the mineral [18,19]. The crystal orientation of fluorite was identified using surface XRD analysis. The (111) surface was the dominant cleavage plane and was most commonly exposed during crushing and grinding (Fig. 1). Therefore, the (111) surface of fluorite was used in the simulated surface reaction system, where the computed fluorite surface represented the nature of the fluorite structure to ensure that the calculation parameter settings were valid and reasonable. The calculation model was established based on the

lattice parameters reported by SPEZIALE and DUFFY [20], which has been widely referenced. All the DFT-based simulation calculations were performed using the Dmol3 package in Material Studio 2019 (Accelrys Inc.). The geometric crystal parameters and total energy of the fluorite bulk in the DFT simulations were based on the assumption that the free surface was the most stable cleavage plane, i.e. (111), and the OHA collector, adsorbed collector, and calcite supernatant species on the mineral surface were evaluated.

Generalized-gradient approximation with Perdew–Burke–Ernzerhof for solid (GGA-PBESol) exchange–correlation functional has yielded DFT simulation calculation results that closely reflect experimental results [21]. Thus, the GGA-PBESol exchange–correlation functional was used to describe the exchange–correlation interactions. Spin unrestricted calculations of the periodic fluorite slab were considered due to the effect of spin polarization on the energy of adsorption [22]. The core electrons were analyzed using DFT semi-core pseudopotentials and the electronic eigenstates were developed on a double numerical plus polarization basis, where a medium orbital cut-off radius was used. A self-consistent field tolerance of  $2.0 \times 10^{-6}$  Ha/atom was used, and the convergence criteria for the energy, maximum force, and maximum displacement were  $2 \times 10^{-5}$  Ha,  $0.05$  Ha/Å, and  $0.002$  Å, respectively. Smearing was set to be  $5 \times 10^{-3}$  in all calculations, and other parameters were default settings. These parameters were selected according to previous DFT research [6,12,23].

The most stable cleavage plane of fluorite, i.e. (111), was used. All the mineral surface calculations were conducted for surfaces with a (3×3) surface unit cell and a thickness of two layers, thus giving a total of 68 substrate atoms in the unit cell. A vacuum region of  $\sim 40$  Å prevented electronic interactions between adjacent periodic replica perpendicular to the surfaces. The flotation process was performed in an aqueous environment, and thus, the adsorption behavior of the reagents was significantly affected by water molecules [24,25]. The accuracy of the calculation model was ensured by performing all simulation calculations with a conductor-like screening model (COSMO) as an implicit solvation model, using water as the solvent in which the solute molecules formed cavities (dielectric continuum of permittivity of 78.54) [17].

Only upper layer fluorite surface atoms interacted with the OHA collector and the other species. Thus, the adsorption calculations involving either the collector or calcite supernatant species on the fluorite surfaces were based on the assumption that only the atoms in the upper layer were allowed to relax, and the atoms in the sub-layer were constrained in the lattice positions of the fluorite crystal. The adsorption energies of the collector and adsorbed calcite species on the fluorite surfaces were calculated according to [24]

$$E_{\text{ad}} = E_{(\text{slab} + \text{OHA or adsorbed species})} - E_{(\text{slab})} - E_{(\text{OHA or adsorbed species})} \quad (1)$$

where  $E_{\text{ad}}$  is adsorption energy,  $E_{(\text{slab} + \text{OHA or adsorbed species})}$  is total energy of the collector or adsorbed calcite species on the fluorite surface after adsorption,  $E_{(\text{slab})}$  is the total energy of the relaxed bare fluorite slab, and  $E_{(\text{OHA or adsorbed species})}$  is the energy of the OHA ions or adsorbed calcite species after optimization. All energies were measured as kilojoules per mole (kJ/mol), and a negative value indicates exothermic adsorption. The DFT adsorption energy after the OHA collector and adsorbed calcite species interacted with the fluorite surface was calculated according to [26]

$$E_{\text{ad}} = E_{(\text{slab} + \text{OHA} + \text{adsorbed species})} - E_{(\text{slab} + \text{adsorbed species})} - E_{(\text{OHA})} \quad (2)$$

where  $E_{(\text{slab} + \text{adsorbed species})}$  is total energy of fluorite slab and adsorbed calcite species, and  $E_{(\text{OHA})}$  is the energy of the OHA ions.

## 3 Results

### 3.1 Microflotation

The effects of OHA concentration and pH on the floatability of single minerals in the common fluorite flotation system are illustrated in Figs. 2 and 3, respectively. The recovery of fluorite and calcite reached (94.6±0.8)% and (89.1±3.8)%, respectively, using the optimal OHA collector concentration of 0.3 mol/L at a pH of 9. Furthermore, calcite and fluorite exhibited similar floatability in weak alkaline.

The effects of the dissolved calcite species on mineral floatability were evaluated based on the microflotation testing of fluorite and calcite in the presence of calcite supernatant. The fluorite recovery decreased dramatically from (94.6±0.8)% to (40.6±1.4)% when the calcite supernatant was

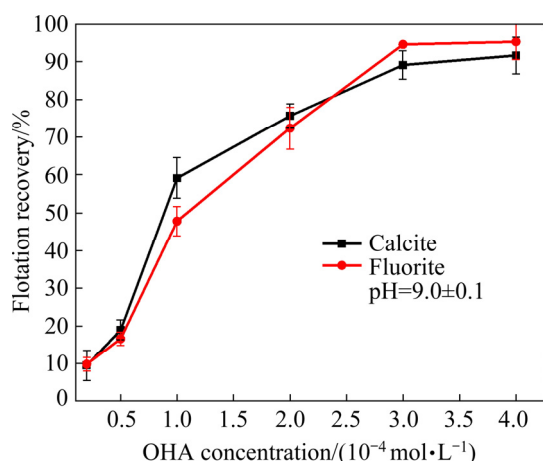


**Fig. 2** Effect of octanohydroxamic acid (OHA) concentration on mineral flotation recovery at pH 9 (The error bars represent the 95% confidence interval)

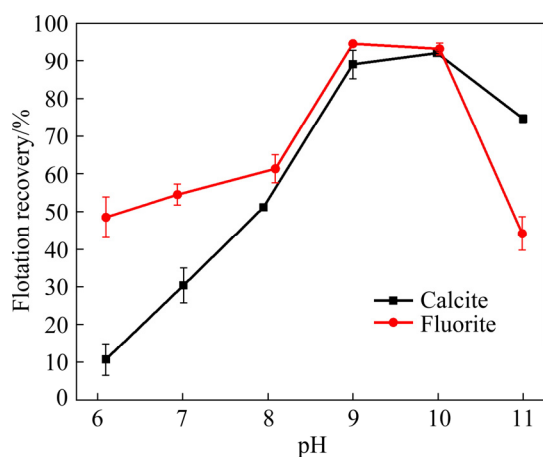


**Fig. 3** Effect of pH on mineral flotation recovery (Octanohydroxamic acid concentration is 0.3 mmol/L; error bars represent the 95% confidence interval)

used instead of pure water (Fig. 4). Thus, the calcite supernatant affected the adsorption of OHA onto the surface of fluorite. However, the calcite recovery was less affected, and only decreased from (89.1±3.8)% to (70.3±8.1)%. A previous study attributed this change in calcite recovery to the interaction between the collector and calcium ions, and collector concentration in solution [6,13,27].

### 3.2 FTIR spectra analysis

The mechanism through which the calcite species affected the adsorption of OHA on the fluorite surface was evaluated based on FTIR spectra of untreated fluorite, fluorite treated with OHA alone, and fluorite treated with OHA in calcite supernatant (Fig. 5). Furthermore, the infrared spectrum of OHA is given in Fig. 6. OHA exhibited

absorption bands at ~3258, 2916, and 2846 cm<sup>-1</sup>, which were attributed to stretching vibrations of N—H, C—H in —CH<sub>3</sub>, and C—H in —CH<sub>2</sub>—, respectively (Fig. 6) [28]. The peak at ~1663 cm<sup>-1</sup> was characteristic peak of stretching vibrations in the C=O group (carbonyl) of OHA, whereas that at ~1423.9 cm<sup>-1</sup> was associated with —N—O—H in-plane bending. The broad peak spanning from 1300 to 1100 m<sup>-1</sup> was attributed to C—N stretching vibration. The peak at ~1053 cm<sup>-1</sup> was attributed to C—O stretching vibrations [29,30], indicating the presence of contaminants (e.g., calcite).

Absorption at ~3500 and 1600 cm<sup>-1</sup> was attributed to water adsorbed during sample preparation (Fig. 6). Fluorite sample treated with OHA exhibited peaks at 2978.0 and 2901.8 cm<sup>-1</sup>, which confirmed that OHA was adsorbed on the

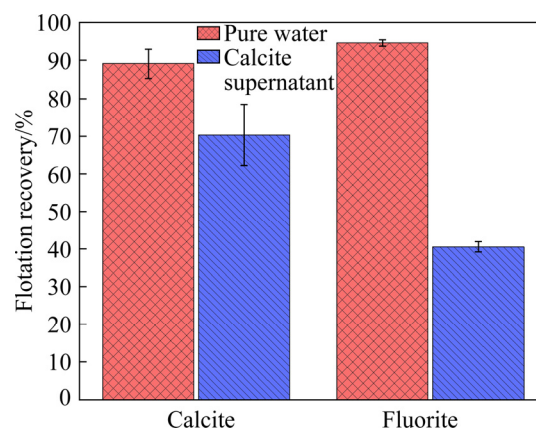


**Fig. 4** Microflotation recovery of calcite and fluorite using octanohydroxamic acid collector (0.3 mmol/L) in ultrapure water and calcite supernatant (pH=9) (Error bars represent the 95% confidence interval)

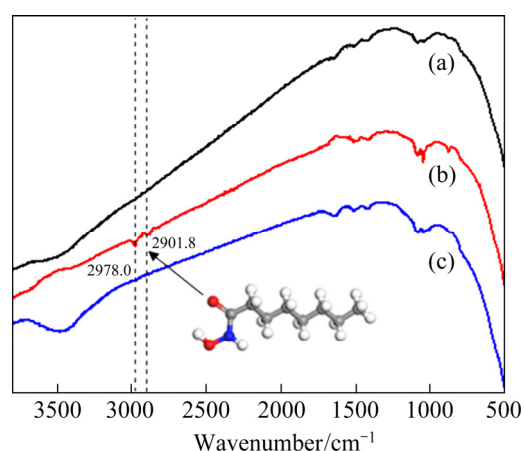


**Fig. 5** Fourier transform infrared spectra of pure fluorite (a), fluorite treated with OHA (b), and fluorite treated with octanohydroxamic acid in calcite supernatant (c)

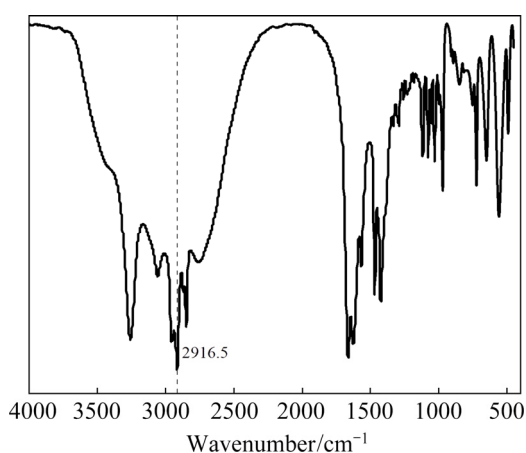


**Fig. 6** Fourier transform infrared spectrum of octanohydroxamic acid

fluorite surface via chemical bonding (Fig. 5(b)). The fluorite treated with OHA in the calcite supernatant exhibited substantial weakening of the characteristic stretching vibration peak at  $\sim 2916$ , and  $2846\text{ cm}^{-1}$  of C—H in OHA (Fig. 5(c)) [31]. These observations indicated that the adsorption of OHA on the fluorite was suppressed by the presence of the calcite species, which confirms with the findings of the microflotation experiments.

### 3.3 Solution chemistry calculations

The possible species adsorbed on the fluorite surface due to calcite dissolution were determined using solution chemistry analysis. The calcite supernatant predominantly contained  $\text{CaCO}_3$  due to the thermal stability of carbonate anions at a pH of 9. The species distribution diagrams of calcium and OHA species in an aqueous solution are presented in Fig. 7, where the total concentrations of  $\text{Ca}^{2+}$  ions and OHA used in the solution chemistry calculations were 0.1 and 0.3 mmol/L, respectively, and the relevant chemical reactions and equilibrium constants are listed in Table 2 [32].  $\text{Ca}^{2+}$  was the principal calcium species in an aqueous solution at a pH of 9 (Fig. 7(a)). Furthermore, a large amount of  $\text{CaCO}_3$  precipitated under these pH conditions [33]. The OHA anions co-existed with OHA molecules in an aqueous solution at a pH of 9 (Fig. 7(b)). However, previous studies have shown that hydroxamic acid collector ions are more readily adsorbed on minerals rather than the collector molecule [16,34]. Thus, the DFT simulations only considered deprotonated OHA to avoid redundancy.

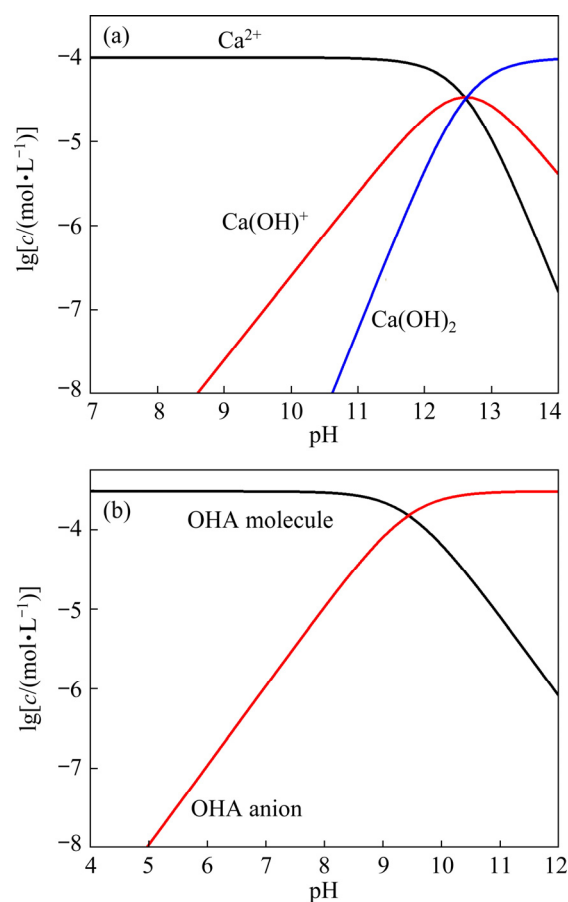


**Fig. 7** Species distributions for  $\text{Ca}^{2+}$  (0.1 mmol/L) (a) and octanohydroxamic acid (0.3 mmol/L) (b)

**Table 2** Pertinent chemical reactions and equilibrium constants for calcite and oleate solution chemistry calculations

Reaction	Equilibrium constant
$\text{H}_2\text{O} \rightleftharpoons \text{H}^+ + \text{OH}^-$	$K_{\text{W}} = 10^{-14}$
$\text{CaCO}_{3(\text{s})} = \text{Ca}^{2+} + \text{CO}_3^{2-}$	$K_{\text{sp}1} = 10^{-8.35}$
$\text{Ca}^{2+} + \text{OH}^- = \text{Ca}(\text{OH})^+$	$K_1 = 10^{-1.4}$
$\text{Ca}(\text{OH})^+ + \text{OH}^- = \text{Ca}(\text{OH})_2$	$K_2 = 10^{2.77}$
$\text{Ca}(\text{OH})^+ + \text{OH}^- = \text{Ca}(\text{OH})_{2(\text{s})}$	$K_{\text{sp}2} = 10^{5.22}$
$\text{OHA}_{(\text{aq})} \rightleftharpoons \text{OHA}^- + \text{H}^+$	$K_{\text{im}} = 10^{-9.44}$

### 3.4 XPS analysis

The XPS spectra of the fluorite treated with ultrapure water, ultrapure water and OHA, supernatant, and supernatant and OHA were analyzed to study the adsorption of calcite species at the fluorite surface. Changes in the chemical surroundings of C, O, and N at the mineral surface were determined using the unprocessed and peak-fitted high-resolution XPS spectra (Figs. 8 and

9). The C 1s spectra of fluorite treated with ultrapure water alone exhibited peaks at  $\sim 284.8$ , 286.5 and 288.6 eV (Fig. 8(a<sub>1</sub>)), which were assigned to the C—C, C—O, and C=O units of adventitious carbon, respectively. Further, the O 1s signals at  $\sim 531.9$  eV (Fig. 8(b<sub>1</sub>)) were assigned to C=O [35]. These species were considered as contamination. Treatment with OHA alone caused a shift in the C—O and C=O peaks of +0.3 and +0.2 eV to  $\sim 286.8$  and 288.8 eV, respectively (Fig. 8(a<sub>2</sub>)) [30,36]. The C=O peak in the O 1s

spectra exhibited a weak shift of +0.1 eV to  $\sim 532.0$  eV (Fig. 8(b<sub>2</sub>)), and a new peak was observed at  $\sim 531.0$  eV and was assigned to N—O [37,38]. These results indicated that OHA was adsorbed on the fluorite surface in the absence of the calcite supernatant. The C 1s spectra of the fluorite treated with the calcite supernatant alone exhibited a peak at  $\sim 288.7$  eV (Fig. 8(a<sub>3</sub>)), which confirmed the presence of CaCO<sub>3</sub> [39]. Thus, the calcite species was adsorbed on the fluorite surface. Consequently, the C—O peak shifted by  $-0.2$  to

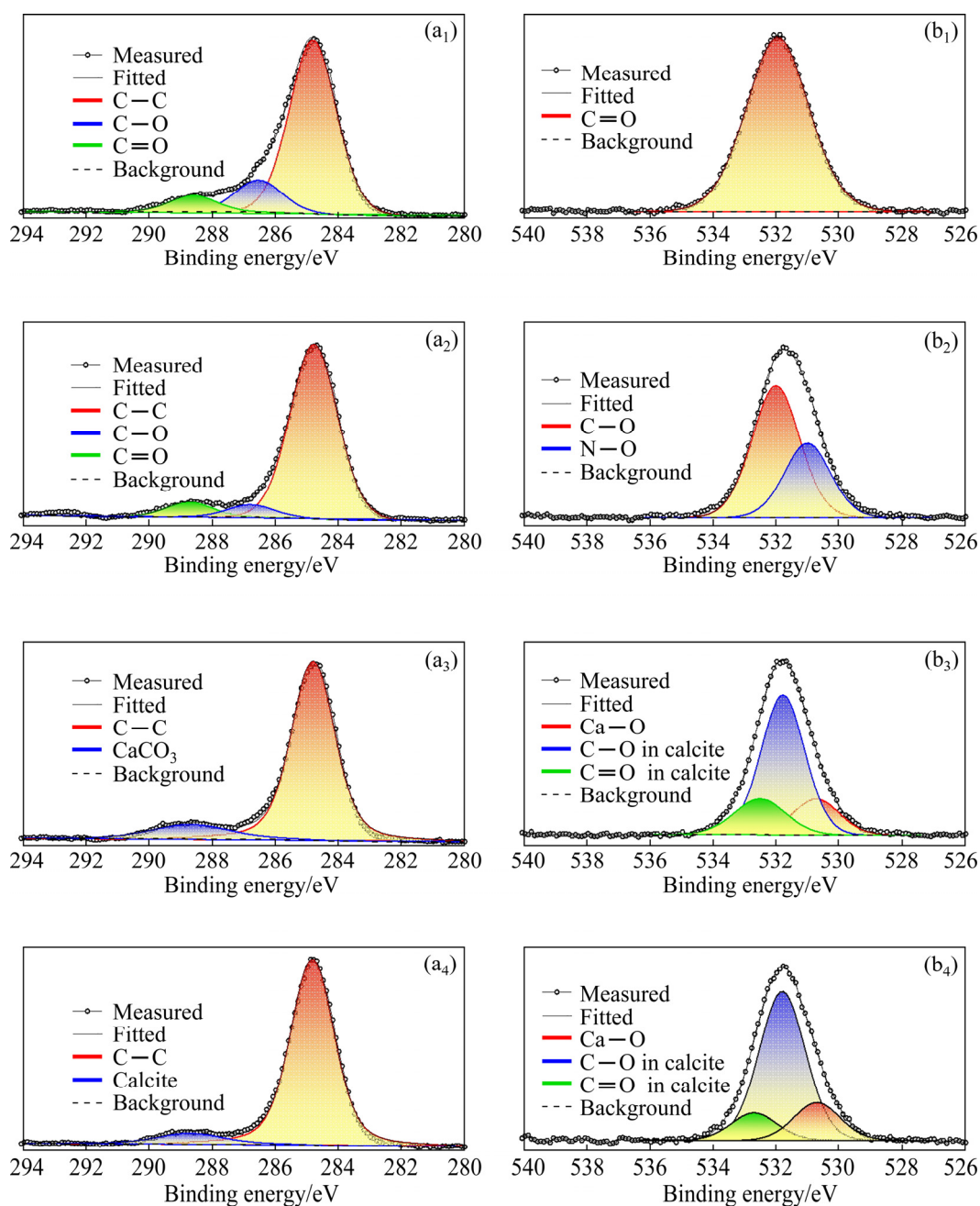


**Fig. 8** Unprocessed and fitted high-resolution C 1s and O 1s spectra of fluorite treated with ultrapure water (a<sub>1</sub>, b<sub>1</sub>), ultrapure water and octanohydroxamic acid (OHA) (a<sub>2</sub>, b<sub>2</sub>), supernatant (a<sub>3</sub>, b<sub>3</sub>) and supernatant and OHA (a<sub>4</sub>, b<sub>4</sub>) (pH=9)

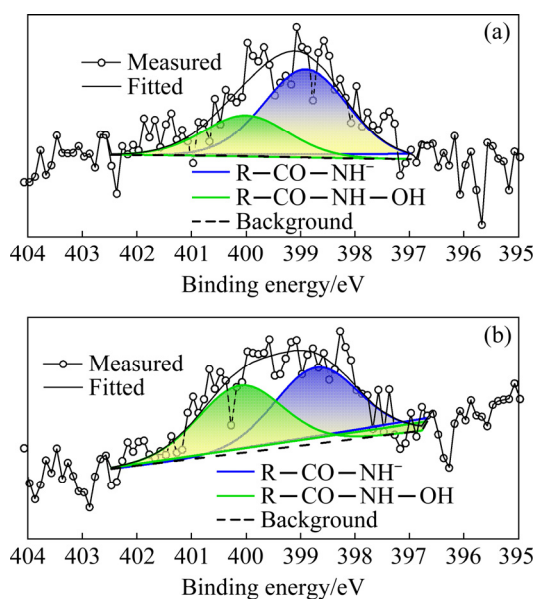


**Fig. 9** Unprocessed and fitted high-resolution N 1s spectra of fluorite treated with octanohydroxamic acid (OHA) (a) and supernatant and OHA (b) (pH = 9)

~531.8 eV (Fig. 8(b<sub>3</sub>)) due to a change in the chemical surroundings of O on the fluorite surface. Thus, the peaks at ~531.8 and 532.5 eV of the O 1s spectra were assigned to C—O and C=O in calcite [40]. Similarly, the peak at ~530.7 eV was attributed to Ca—O from calcium carbonate polymorphs [41]. The samples treated with OHA after contacting with the supernatant did not exhibit any new peaks in the C 1s spectra (Fig. 8(a<sub>4</sub>)), thus indicating that OHA adsorption was primarily inhibited by the presence of the calcite supernatant. A slight change of C=O chemical surrounds (+0.2 eV) further suggested that the adsorption of OHA was severely suppressed, but was not inhibited completely.

The N 1s XPS spectra of fluorite treated with OHA alone, and OHA after exposure to the calcite supernatant are given in Fig. 9. The XPS spectra of N 1s were fitted to two peaks at ~398.7 eV, which was assigned to N in the deprotonated hydroxamate groups (R—CO—NH—O—), and ~399.9 eV, which was attributed to N in neutral molecules [42], i.e. the protonated form of the hydroxamic acid (R—CO—NH—OH) [43,44]. The first step in the chemisorption of hydroxamic acid on the mineral surface was deprotonation [45]. Thus, the peak at ~398.7 eV was attributed to the chemical adsorption of OHA, while the peak at ~399.9 eV was caused by the physical adsorption of OHA. The chemically

adsorbed OHA (Fig. 9(a)) was the primary adsorption form (~70%) in the presence OHA alone, but the adsorption ratio of deprotonated OHA on the fluorite surface sharply decreased to ~50% after treatment with the calcite supernatant. This weak interaction between the OHA and the fluorite surface lowered the floatability of fluorite.

### 3.5 DFT computational results

The FTIR and XPS spectra provided insights into the adsorption events between the fluorite surface and the calcite supernatant species. However, these analyses did not illustrate the nature of these interactions, nor the mechanism through which the adsorbed species inhibited OHA adsorption. DFT calculations were used to simulate the interaction of OHA<sup>-</sup> on the fluorite surface, as well as in the presence of calcite supernatant.

#### 3.5.1 Structural optimization structure of OHA anion

The molecular structure and reactivity of the collector play an important role in its interaction with the mineral surface. Therefore, the DFT optimized structure of the OHA collector is shown in Fig. 10(a). The bond lengths of N—O, C—N, and C=O were approximately 1.314, 1.349, and 1.258 Å, respectively. Valence electron transfer usually occurs at the collector's highest occupied molecular orbital (HOMO). That is, HOMO is the most active orbital, which is thus the most active orbital. Therefore, the HOMO was used to predict the binding sites of the OHA ions [17]. The HOMO

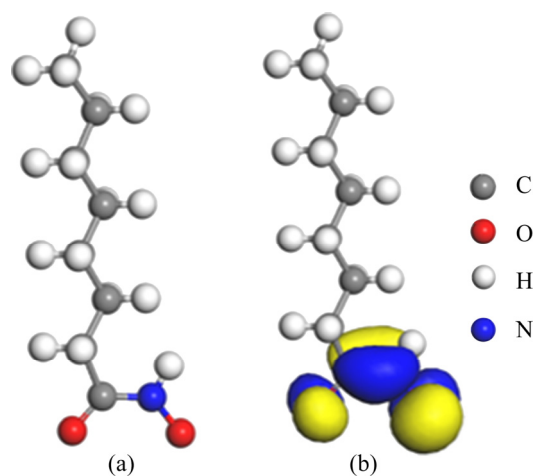


**Fig. 10** Density functional theory optimized structure of anionic form of octanohydroxamic acid (OHA) (a) and highest occupied molecular orbital of anionic OHA collector (b)

of the OHA collector is illustrated in Fig. 10(b), where the transferable valence electron was located around the polar head (C=O and N—O). Mulliken atomic charge analysis revealed negative charges around the two O atoms of the OHA anion, whereas the computational results showed that the charges of O on C=O and N—O were  $-0.602 e$  and  $-0.642 e$ , respectively. Thus, the two O atoms contributed most to the covalent bonding between OHA and metal ion complexes. Specifically, the interaction between the N—O oxygen atom and the metal ions on the mineral surface was likely to form stronger covalent bonding than the C=O bond.

### 3.5.2 Structural optimization of fluorite surface

The (111) surface is considered to be the most stable surface of fluorite, and previous studies have reported that the (111) surface is the dominant cleavage plane due to the electrostatic repulsion between adjacent anion layers [12,46]. This surface was exposed by cleaving the optimized fluorite crystal structures through the (111) plane (Fig. 11). During optimization of surface, all atomic displacements were allowed through relaxation. The upper atoms of the fluorite (111) surface consist of a repeated hexagonal array comprising Ca and F, where each Ca atom is surrounded by eight F atoms and each F atom is surrounded by four Ca atoms. The bonding between Ca and F occurred from both above and below. The deformation charge density map of the fluorite (111) surface (Fig. 12) indicated that the strong electronegativity of F caused a transfer of the electrons around the Ca atoms to the F atoms on the fluorite surface. Thus, the Ca atoms on the fluorite surface were the primary active centers for interaction with the collector. Geometry optimization led to changes due to the upward movement of Ca and F atom positions, where the Ca—F distances in the top hexagonal array increased by  $\sim 0.05 \text{ \AA}$ . Further, the vertical Ca—F distances either increased by  $\sim 0.27 \text{ \AA}$  or decreased by  $\sim 0.20 \text{ \AA}$ .

### 3.5.3 Adsorption of calcite supernatant species on fluorite (111) surface

The solution chemistry calculations indicated that  $\text{CaCO}_3$  and  $\text{Ca}^{2+}$  in the calcite supernatant possibly adsorbed onto the fluorite surface.  $\text{CaCO}_3$  and  $\text{Ca}^{2+}$  located at various initial positions on the fluorite (111) surface were simulated to identify the most common adsorption conformation. The

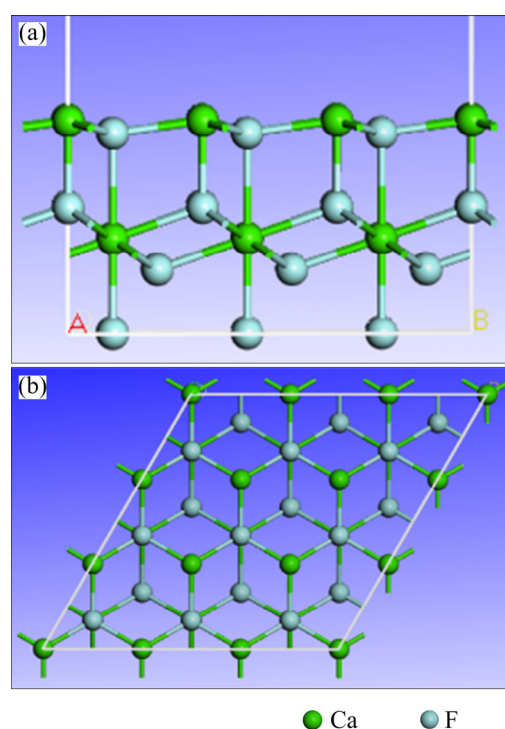


**Fig. 11** Structure of fluorite (111) surface viewed from side (a) and top (b)

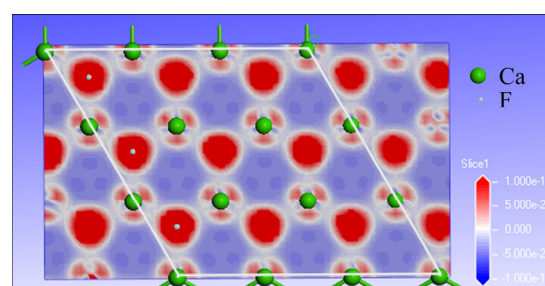


**Fig. 12** Charge density differences for fluorite (111) surface

optimized geometric structures demonstrated that  $\text{Ca}^{2+}$  was not stably adsorbed on the fluorite surface (Fig. 13). The Ca—F bond lengths between the adsorbed  $\text{Ca}^{2+}$  ions and three F atoms in the hexagonal array on the fluorite surface were  $\sim 3.42$ ,  $3.48$ , and  $3.58 \text{ \AA}$ . As  $\text{Ca}^{2+}$  was not stably adsorbed, only the adsorption of  $\text{CaCO}_3$  was considered.

The most stable adsorption configuration of  $\text{CaCO}_3$  is given in Fig. 14, where the Ca—O lengths between the O furthest from Ca in  $\text{CaCO}_3$  and the three Ca atoms in the hexagonal array on the fluorite surface were  $\sim 2.27$ ,  $2.28$ , and  $2.28 \text{ \AA}$ . Ca atoms on the fluorite surface were exposed on the top layer. However, the F atoms facilitated easier adsorption of  $\text{CaCO}_3$  from calcite supernatant onto the fluorite surface. The adsorption of  $\text{CaCO}_3$

on the fluorite surface was highly favorable with a calculated adsorption energy of  $-608.2$  kJ/mol. Further, a new active site for OHA collector adsorption was likely formed due to the adsorption of metal ion species [6].

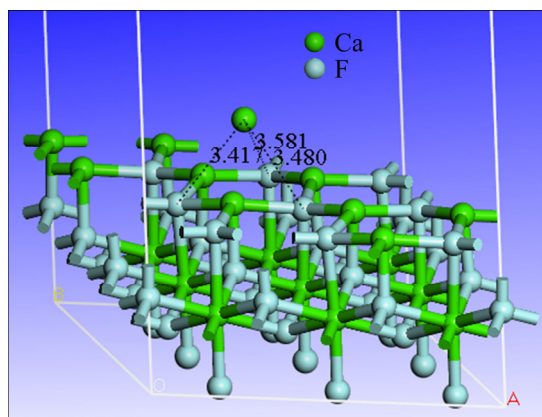


**Fig. 13** Interaction of Ca ions on fluorite surface (111) (Unit: Å)

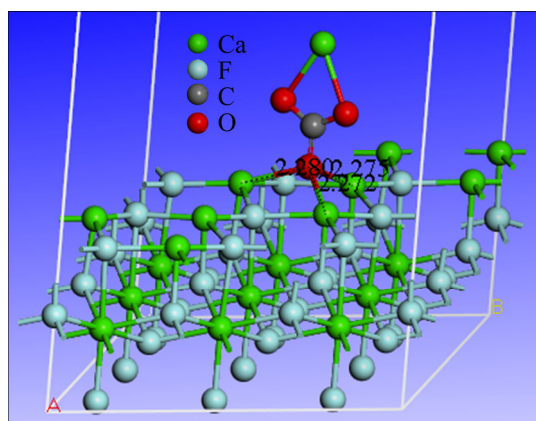


**Fig. 14** Interaction between  $\text{CaCO}_3$  and fluorite (111) surface (Unit: Å)

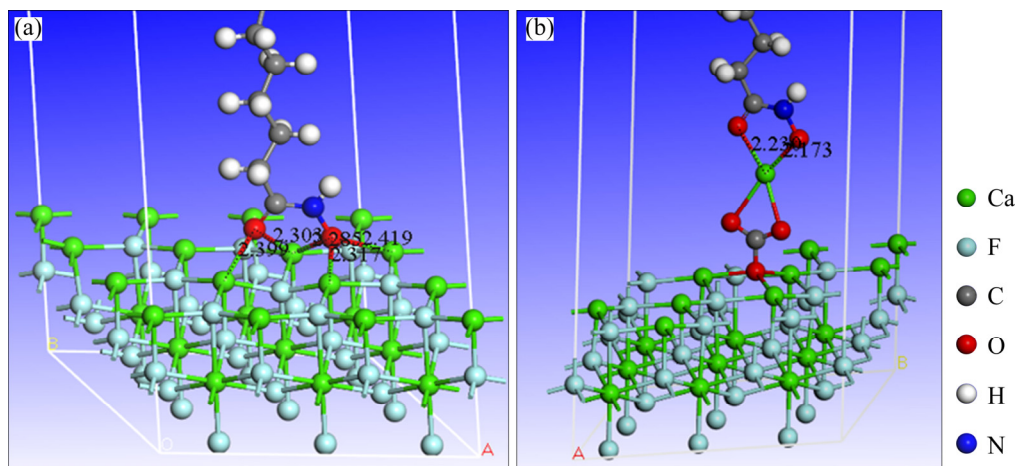


**Fig. 15** Interaction between fluorite surface and octanohydroxamic acid without supernatant species (a) and with  $\text{CaCO}_3$  on fluorite (111) surface (b) (Unit: Å)

### 3.5.4 Effect of calcite supernatant species of adsorption of OHA on fluorite (111) surface

The differences in fluorite flotation behavior in ultrapure water or calcite supernatant were investigated based on the interaction between OHA and the fluorite surfaces using DFT simulation calculation. A detailed illustration of the interaction between the conjugate base of OHA and the bare fluorite surfaces is given in Fig. 15(a).

The adsorption of OHA on the fluorite surface in the absence of calcite supernatant species was similar to the phenomena discussed earlier. The polar head of OHA had a high potential to interact with the mineral surfaces due to the HOMO transferable charges located in the functional groups of  $-\text{C}(=\text{O})-\text{NH}-\text{O}-$ . One of the two O polar heads in OHA is bonded with three Ca atoms, and the other is connected with two Ca atoms in the adjacent hexagonal arrays. This phenomenon differs slightly from existing knowledge, where it was previously considered that hydroxamic acid type collectors exhibit chemisorption with the mineral surface in both monodentate and bidentate (the stable five-membered ring structure) forms. The O atoms in the  $\text{N}-\text{O}$  and  $\text{C}=\text{O}$  groups interact with Ca atoms on the fluorite surface via covalent bonding (Fig. 15(a)). The  $\text{Ca}-\text{O}$  lengths between the  $\text{N}-\text{O}$  groups and the three Ca in the hexagonal array on the fluorite surface were  $\sim 2.28$ ,  $2.32$ , and  $2.42$  Å, whereas those between  $\text{C}=\text{O}$  groups and the two Ca atoms in adjacent hexagonal arrays were  $\sim 2.30$  and  $2.40$  Å, respectively. Similarly, high adsorption energy ( $-533.56$  kJ/mol) was calculated for this bridged binding form using Eq. (1). Overall,

the findings indicate that OHA had a strong collection capacity for fluorite in ultrapure water; however, its adsorption was weaker than  $\text{CaCO}_3$ .

The pre-adsorption of calcite species covered active sites on the fluorite surface. Subsequent adsorption of OHA at the active sites adjacent to the adsorbed calcite species caused strong steric hindrance. As discussed in Section 3.5.3, the pre-formed precipitates could serve as new adsorption sites on the fluorite surface. Thus, the adsorption of OHA (deprotonation) over the pre-adsorbed  $\text{CaCO}_3$  on the fluorite surface was investigated, and the optimized geometry structures are shown in Fig. 15(b). The polar head group of OHA interacted with  $\text{Ca}^{2+}$  from the pre-adsorbed calcite species via bidentate chemisorption. The C=O or N—O groups of OHA interacted with the Ca atom in  $\text{CaCO}_3$  via covalent bonding (Fig. 15(a)). The Ca—O distances between the Ca atoms in  $\text{CaCO}_3$  and the C=O and N—O groups in this configuration were  $\sim 2.23$  and  $2.17$  Å, respectively. The OHA adsorption energy decreased significantly to  $-236.48$  kJ/mol once the fluorite surface comprised pre-adsorbed collector-interacting  $\text{Ca}^{2+}$  from  $\text{CaCO}_3$  in the calcite supernatant. Thus, the interaction between OHA and fluorite was weak.

## 4 Discussion

The calcite supernatant significantly affected the floatability of fluorite, as demonstrated in the microflotation testing. The surface properties of fluorite were affected by the adsorption of calcite species, as confirmed by FTIR, solution chemistry, and XPS analyses. Previous studies have reported that calcite species affect fluorite floatability due to the interaction between the collector and dissolved species. A large proportion of the OHA collector was consumed by the  $\text{Ca}^{2+}$  ions from calcite dissolution [13,14]. The flotation recovery of calcite in the calcite supernatant also decreased slightly. Solution chemistry analysis indicated that  $\text{CaCO}_3$  and  $\text{Ca}^{2+}$  might be preferentially adsorbed on the fluorite surface. The adsorption of the calcite species was not explicitly observed in the FTIR spectra acquired at a pH of 9 (Fig. 5). However, the differences between the fluorite samples after the addition of OHA with and without calcite supernatant confirmed that the added calcite

supernatant hindered the adsorption of OHA on the fluorite surface.

DFT simulations further confirmed that the  $\text{CaCO}_3$ –fluorite interaction was favored over OHA–fluorite interactions. Thus,  $\text{CaCO}_3$  was preferentially adsorbed on the fluorite surface instead of OHA. Further, pre-adsorption of  $\text{CaCO}_3$  on the fluorite surface caused strong steric hindrance, which prevented the adsorption of OHA. Although new active sites were formed due to the adsorption of  $\text{CaCO}_3$ , this steric hindrance prevented effective OHA adsorption. Le Chatelier's principle dictates that an increase in reactant concentration would disturb the system and increase the rate of the forward reaction until the equilibrium state is achieved. Thus, the addition of reactants would promote the formation of  $\text{CaCO}_3$  precipitates on the fluorite surface, further increasing the steric hindrance [6].  $\text{Ca}^{2+}$  ions were not stably adsorbed on the fluorite surface due to the positively charged  $\text{Ca}^{2+}$  layer on the top layer of the fluorite surface, which caused electrostatic repulsion. Previous studies have reported similar observations [47,48]. The XPS spectra confirmed the presence of  $\text{CaCO}_3$  on the fluorite surface (Fig. 8). This was likely contributed by two sources, namely  $\text{CaCO}_3$  from direct adsorption of the calcite supernatant on the fluorite surface, and  $\text{Ca}^{2+}$  at the fluorite surface interacting with the  $\text{CO}_3^{2-}$  ions in solution (Table 2). Thus, introducing  $\text{CO}_3^{2-}$  ions into the solution hindered the adsorption of OHA due to the common ion effect [49–51].

It is widely accepted that the most stable adsorption configuration is the configuration with the lowest total energy [52]. The optimized adsorption geometry configuration of OHA on the fluorite surface was not the bidentate. Electron transfer and a higher density of  $\text{Ca}^{2+}$  ions led to the formation of a vacant valence electron shell of  $\text{Ca}^{2+}$  ions on the fluorite surface (Fig. 11) [12]. The O atoms in the N—O and C=O groups interact with three and two Ca atoms on the fluorite surface via covalent bonding, respectively. Thus, a stable octet configuration was formed for all atoms participating in the adsorption.

## 5 Conclusions

(1) The flotation recovery of fluorite was significantly decreased from 94.6% to 40.6% by

calcite dissolved species. FTIR spectra and XPS analysis showed that the adsorption of OHA on the fluorite was decreased in the presence of the calcite dissolved species, and the weaker interaction was observed between the OHA and the fluorite surface.

(2) DFT computation results indicated that  $\text{CaCO}_3$  was more stably adsorbed on the fluorite surface than  $\text{Ca}^{2+}$ . The adsorption energy of  $\text{CaCO}_3$  on the fluorite surface was higher than that of OHA, indicating that  $\text{CaCO}_3$  was preferentially adsorbed over multidentate OHA. The pre-adsorption of  $\text{CaCO}_3$  led to the formation of active sites on the  $\text{Ca}^{2+}$  of the adsorbed  $\text{CaCO}_3$ . However, OHA adsorption at these new sites was not favorable.

(3) This study presents a novel suggestion that the adsorption configuration of OHA on the fluorite (111) surface was the multidentate form, and not the bidentate. This configuration allows for a more stable octet for all atoms participating in the adsorption.

(4) This work provides valuable insights into the selection and synthesis of collectors in flotation systems. Preventing the effects of the gangue species in fluorite flotation should be further investigated to improve the recovery and grade of fluorite.

## Acknowledgments

The authors are grateful for the financial supports from the National Natural Science Foundation of China (Nos. 51874247, 51922091, 51904249), Young Elite Scientists Sponsorship Program by CAST, China (No. 2018QNRC001), Sichuan Science and Technology Program, China (Nos. 2019YFS0453, 2018JY0148), Open Research Fund of State Key Laboratory of Complex Nonferrous Metal Resources Clean Utilization, China (No. CNMRCUKF2001), and Postgraduate Innovation Fund by Southwest University of Science and Technology, China (No. 20ycx0027).

## References

- [1] LIU Cheng, SONG Shao-xian, LI Hong-qiang. Selective flotation of fluorite from barite using trisodium phosphate as a depressant [J]. *Minerals Engineering*, 2019, 134: 390–393.
- [2] CHEN Wei, CHEN Yao, BU Xian-zhong, LONG Tao, ZHANG Guo-fan, CHEN Fan-fan, LIU Run-zhe, JIA K, SONG Y. Rheological investigations on the hetero-coagulation between the fine fluorite and quartz under fluorite flotation-related conditions [J]. *Powder Technology*, 2019, 354: 423–431.
- [3] WILLS B A, FINCH J A. Chapter 12–Froth flotation [M]/Wills' Mineral Processing Technology. BosMg: Butterworth-Heinemann, 2016: 265–380.
- [4] FANG Shuai, XU Long-hua, WU Hou-qin, SHU Kai-qian, XU Yan-bo, ZHANG Zhen-yue, CHI Ru-an, SUN Wei. Comparative studies of flotation and adsorption of Pb(II)/benzohydroxamic acid collector complexes on ilmenite and titanite [J]. *Powder Technology*, 2019, 345: 35–42.
- [5] REN Liu-yi, QIU Hang, ZHANG Ming, FENG Kai-yue, LIU Peng, GUO Jing, FENG Jian. The behavior of lead ions in cassiterite flotation using octanohydroxamic acid [J]. *Industrial & Engineering Chemistry Research*, 2017, 56(30): 8723–8728.
- [6] ESPIRITU E R L, DA SILVA G R, AZIZI D, LARACHI F, WATERS K E. The effect of dissolved mineral species on bastnaesite, monazite and dolomite flotation using benzohydroxamate collector [J]. *Colloids and Surfaces A: Physicochemical and Engineering Aspects*, 2018, 539: 319–334.
- [7] GAO Zhi-yong, WANG Cong, SUN Wei, GAO Yue-sheng, KOWALCZUK P B. Froth flotation of fluorite: A review [J]. *Advances in Colloid and Interface Science*, 2021, 290: 102382.
- [8] HU Yue-hua, CHI Ru-an, XU Zheng-he. Solution chemistry study of salt-type mineral flotation systems: Role of inorganic dispersants [J]. *Industrial & Engineering Chemistry Research*, 2003, 42(8): 1641–1647.
- [9] ZHU Hai-ling, QIN Wen-qing, CHEN Chen, CHAI Li-yuan, JIAO Fen, JIA Wen-hao. Flotation separation of fluorite from calcite using polyaspartate as depressant [J]. *Minerals Engineering*, 2018, 120: 80–86.
- [10] FENG Bo, LUO Xian-ping, WANG Jin-pin, WANG Peng-cheng. The flotation separation of scheelite from calcite using acidified sodium silicate as depressant [J]. *Minerals Engineering*, 2015, 80: 45–49.
- [11] SALMANI NURI O, IRANNAJAD M, MEHDILO A. Effect of surface dissolution on kinetic parameters in flotation of ilmenite from different gangue minerals [J]. *Transactions of Nonferrous Metals Society of China*, 2019, 29(12): 2615–2626.
- [12] JIANG Wei, GAO Zhi-yong, KHOSO S A, GAO Jian-de, SUN Wei, PU Wei, HU Yue-hua. Selective adsorption of benzohydroxamic acid on fluorite rendering selective separation of fluorite/calcite [J]. *Applied Surface Science*, 2018, 435: 752–758.
- [13] WANG Zhou-jie, WU Hou-qin, XU Yan-bo, SHU Kai-qian, FANG Shuai, XU Long-hua. The effect of dissolved calcite species on the flotation of bastnaesite using sodium oleate [J]. *Minerals Engineering*, 2020, 145: 106095.
- [14] WANG Zhou-jie, WU Hou-qin, XU Yan-bo, SHU Kai-qian, YANG Jie, LUO Li-ping, XU Long-hua. Effect of dissolved fluorite and barite species on the flotation and adsorption behavior of bastnaesite [J]. *Separation and Purification Technology*, 2020, 237: 116387.
- [15] QUEZADA G R, TOLEDO P G. Structure of the interface between lithium-rich spodumene and saltwater by density functional theory calculations and molecular dynamics

- simulations [J]. *The Journal of Physical Chemistry C*, 2019, 124(2): 1446–1457.
- [16] ZHAO Gang, ZHONG Hong, QIU Xian-yang, WANG Shuai, GAO Yu-de, DAI Zi-lin, HUANG Jian-ping, LIU Guang-yi. The DFT study of cyclohexyl hydroxamic acid as a collector in scheelite flotation [J]. *Minerals Engineering*, 2013, 49: 54–60.
- [17] LI Yu-qiong, LIU Ying-chao, CHEN Jian-hua, ZHAO Cui-hua. Structure-activity of chelating collectors for flotation: A DFT study [J]. *Minerals Engineering*, 2020, 146: 106133.
- [18] GAO Zhi-yong, HU Yue-hua, SUN Wei, DRELICH J W. Surface-charge anisotropy of scheelite crystals [J]. *Langmuir*, 2016, 32(25): 6282–6288.
- [19] XU Long-hua, PENG Tie-feng, TIAN Jia, LU Zhong-yuan, HU Yue-hua, SUN Wei. Anisotropic surface physicochemical properties of spodumene and albite crystals: Implications for flotation separation [J]. *Applied Surface Science*, 2017, 426: 1005–1022.
- [20] SPEZIALE S, DUFFY T S. Single-crystal elastic constants of fluorite (CaF<sub>2</sub>) to 9.3 GPa [J]. *Physics Chemistry of Minerals*, 2002, 29(7): 465–472.
- [21] CAO Shi-ming, CAO Yi-jun, MA Zi-long, LIAO Yin-fei, ZHANG Xiao-lin. Structural and electronic properties of bastnaesite and implications for surface reactions in flotation [J]. *Journal of Rare Earths*, 2020, 38(3): 332–338.
- [22] JI Wen-chao, SHEN Zhe-min, FAN Mao-hong, SU Ping-ru, TANG Qing-li, ZOU Cong-yang. Adsorption mechanism of elemental mercury (Hg<sup>0</sup>) on the surface of MnCl<sub>2</sub> (110) studied by density functional theory [J]. *Chemical Engineering Journal*, 2016, 283: 58–64.
- [23] REN Zi-jie, YU Fu-tao, GAO Hui-min, CHEN Zhi-jie, PENG Yong-jun, LIU Ling-yun. Selective separation of fluorite, barite and calcite with valonea extract and sodium fluosilicate as depressants [J]. *Minerals*, 2017, 7(2): 24.
- [24] LIU Meng, CHEN Jian-hua, CHEN Ye, ZHU Yang-ge. Interaction between smithsonite and carboxyl collectors with different molecular structure in the presence of water: A theoretical and experimental study [J]. *Applied Surface Science*, 2020, 510: 145410.
- [25] LIU Jian, ZENG Yong, EJTEMAEI M, NGUYEN A V, WANG Yu, WEN Shu-ming. DFT simulation of S-species interaction with smithsonite (001) surface: Effect of water molecule adsorption position [J]. *Results in Physics*, 2019, 15: 102575.
- [26] WEI Zhao, SUN Wei, HAN Hai-sheng, CAO Jian, GUI Xia-hui, XING Yao-wen, ZHANG Chen-yang, ZOU Jing-xiang. Enhanced electronic effect improves the collecting efficiency of benzohydroxamic acid for scheelite flotation [J]. *Minerals Engineering*, 2020, 152: 106308.
- [27] LI Zhi-li, RAO Feng, GUO Bao, ZUO Wen-ran, SONG Shao-xian, LÓPEZ-VALDIVIESO A. Effects of calcium ions on malachite flotation with octyl hydroxamate [J]. *Minerals Engineering*, 2019, 141: 105854.
- [28] SHU Kai-qian, XU Long-hua, WU Hou-qin, FANG Shuai, WANG Zhou-jie, XU Yan-bo, ZHANG Zhen-yue. Effects of ultrasonic pre-treatment on the flotation of ilmenite and collector adsorption [J]. *Minerals Engineering*, 2019, 137: 124–132.
- [29] ZHANG Zhang, TENG Chun-ying, ZHOU Kang-gen, PENG Chang-hong, CHEN Wei. Degradation characteristics of dissolved organic matter in nanofiltration concentrated landfill leachate during electrocatalytic oxidation [J]. *Chemosphere*, 2020, 255: 127055.
- [30] SHU Kai-qian, XU Long-hua, WU Hou-qin, TANG Zhen, LUO Li-ping, YANG Jie, XU Yan-bo, FENG Bo. Selective flotation separation of spodumene from feldspar using sodium alginate as an organic depressant [J]. *Separation and Purification Technology*, 2020, 248: 117122.
- [31] SHU Kai-qian, XU Long-hua, WU Hou-qin, XU Yan-bo, WANG Zhou-jie. In situ adsorption of mixed anionic/cationic collectors in a spodumene-feldspar flotation system: Implications for collector design [J]. *Langmuir*, 2020, 36: 8086–8099.
- [32] FANG Shuai, XU Long-hua, WU Hou-qin, XU Yan-bo, WANG Zhou-jie, SHU Kai-qian, HU Yue-hua. Influence of surface dissolution on sodium oleate adsorption on ilmenite and its gangue minerals by ultrasonic treatment [J]. *Applied Surface Science*, 2020, 500: 144038.
- [33] ZHANG W, HONAKER R Q, FROPPO J G. Flotation of monazite in the presence of calcite. Part II: Enhanced separation performance using sodium silicate and EDTA [J]. *Minerals Engineering*, 2018, 127: 318–328.
- [34] MENG Qing-you, FENG Qi-ming, SHI Qing, OU Le-ming. Studies on interaction mechanism of fine wolframite with octyl hydroxamic acid [J]. *Minerals Engineering*, 2015, 79: 133–138.
- [35] WANG Zhou-jie, WU Hou-qin, YANG Jie, TANG Zhen, LUO Li-ping, SHU Kai-qian, XU Yan-bo, XU Long-hua. Selective flotation separation of bastnaesite from calcite using xanthan gum as a depressant [J]. *Applied Surface Science*, 2020, 512: 145714.
- [36] YANG Si-yuan, XU Yan-ling, LIU Cheng, HUANG Ling-yun, HUANG Zhi-qiang, LI Hong-qiang. The anionic flotation of fluorite from barite using gelatinized starch as the depressant [J]. *Colloids and Surfaces A: Physicochemical and Engineering Aspects*, 2020, 597: 124794.
- [37] LIU Jian, EJTEMAEI M, NGUYEN A V, WEN Shu-ming, ZENG Yong. Surface chemistry of Pb-activated sphalerite [J]. *Minerals Engineering*, 2020, 145: 106058.
- [38] LE ROUX F, POSSÉMÉ N, BURTIN P, BARNOLA S, TORRES A. XPS study of a selective GaN etching process using self-limiting cyclic approach for power devices application [J]. *Microelectronic Engineering*, 2020, 228: 111328.
- [39] LAAJALEHTO K, SMART R S C, RALSTON J, SUONINEN E. STM and XPS investigation of reaction of galena in air [J]. *Applied Surface Science*, 1993, 64(1): 29–39.
- [40] LI Fang-xu, ZHOU Xiao-tong, LIN Ri-xiao. Flotation performance and adsorption mechanism of novel 1-(2-hydroxyphenyl)hex-2-en-1-one oxime flotation collector to malachite [J]. *Transactions of Nonferrous Metals Society of China*, 2020, 30(10): 2792–2801.
- [41] TENG Fu-cheng, LIU Qing-xia, ZENG Hong-bo. In situ kinetic study of zinc sulfide activation using a quartz crystal microbalance with dissipation (QCM-D) [J]. *Journal of Colloid and Interface Science*, 2012, 368(1): 512–520.

- [42] LONG Yi, LIU Jian-po, LEI Gang, SI Ying-tao, ZHANG Chang-yin, WEI Deng-cheng, SHI Hong-xu. Progressive fracture processes around tunnel triggered by blast disturbances under biaxial compression with different lateral pressure coefficients [J]. Transactions of Nonferrous Metals Society of China, 2020, 30(9): 2518–2535.
- [43] ALAGTA A, FELHÖSI I, BERTOTI I, KÁLMÁN E. Corrosion protection properties of hydroxamic acid self-assembled monolayer on carbon steel [J]. Corrosion Science, 2008, 50(6): 1644–1649.
- [44] CAO Zhao, CAO Yong-dan, QU Qi-qi, ZHANG Jin-shan, MU Yu-fan. Separation of bastnäsite from fluorite using ethylenediamine tetraacetic acid as depressant [J]. Minerals Engineering, 2019, 134: 134–141.
- [45] NI Xiao, LIU Qi. The adsorption and configuration of octyl hydroxamic acid on pyrochlore and calcite [J]. Colloids and Surfaces A: Physicochemical and Engineering Aspects, 2012, 411: 80–86.
- [46] GONG Gui-chen, WANG Pan, LIU Jie, HAN Yue-xin, ZHU Yi-min. Effect and mechanism of Cu(II) on flotation separation of cassiterite from fluorite [J]. Separation and Purification Technology, 2020, 238: 116401.
- [47] ZHANG Zhi-guo, CAO Yi-jun, MA Zi-long, LIAO Yin-fei. Impact of calcium and gypsum on separation of scheelite from fluorite using sodium silicate as depressant [J]. Separation and Purification Technology, 2019, 215: 249–258.
- [48] CHEN Zhi-jie, REN Zi-jie, GAO Hui-min, ZHENG Ren-ji, JIN Yu-lin, NIU Chun-ge. Flotation studies of fluorite and barite with sodium petroleum sulfonate and sodium hexametaphosphate [J]. Journal of Materials Research and Technology, 2019, 8(1): 1267–1273.
- [49] LÓPEZ-VALDIVIESO A, ROBLEDO-CABRERA A, URIBE-SALAS A. Flotation of celestite with the anionic collector sodium dodecyl sulfate. Effect of carbonate ions [J]. International Journal of Mineral Processing, 2000, 60(2): 79–90.
- [50] BUNKHOLT I, KLEIV R A. Flotation of pyrrhotite and pyrite in saturated CaCO<sub>3</sub> solution using a quaternary amine collector [J]. Minerals Engineering, 2015, 70: 55–63.
- [51] CALDEIRA C L, CIMINELLI V S T, OSSEO-ASARE K. The role of carbonate ions in pyrite oxidation in aqueous systems [J]. Geochimica et Cosmochimica Acta, 2010, 74(6): 1777–1789.
- [52] SARVARAMINI A, LARACHI F, HART B. Collector attachment to lead-activated sphalerite-Experiments and DFT study on pH and solvent effects [J]. Applied Surface Science, 2016, 367: 459–472.

## 方解石组分对辛基异羟肟酸在萤石表面吸附的影响

王周杰<sup>1</sup>, 徐龙华<sup>1,2</sup>, 巫侯琴<sup>1</sup>, 周欢<sup>1</sup>, 蒙金萍<sup>1</sup>, 霍笑梅<sup>1</sup>, 黄凌云<sup>3</sup>

1. 西南科技大学 固体废物处理与资源化教育部重点实验室, 绵阳 621010;
2. 西南科技大学 环境友好能源材料国家重点实验室, 绵阳 621010;
3. 昆明理工大学 复杂有色金属资源清洁利用国家重点实验室, 昆明 650093

**摘要:** 在浮选过程中, 萤石的表面性质经常会受到溶解脉石组分(例如: 方解石)的影响。采用 OHA 作为捕收剂, 对有无方解石上清液时进行微浮选测试。研究表明, 溶解的方解石组分明显影响萤石的浮选行为。FTIR 测试证明, 浮选回收率的下降与 OHA 吸附降低有关。溶液化学分析结果表明, 方解石上清液中的 CaCO<sub>3</sub> 和 Ca<sup>2+</sup>是最有可能被吸附的组分。同时, XPS 分析也证实方解石物种在萤石表面的吸附。DFT 模拟计算提供对 OHA 的多齿吸附构型的详细分析, 该构型是 OHA 在萤石表面吸附的最佳构型。计算出的吸附能表明, 与 OHA 相比, 方解石溶解物更稳定地吸附在萤石表面, 而预吸附的方解石溶解组分会通过静电排斥作用阻碍 OHA 的吸附。

**关键词:** 萤石; 方解石; 浮选; 溶解组分; DFT 计算

(Edited by Bing YANG)